

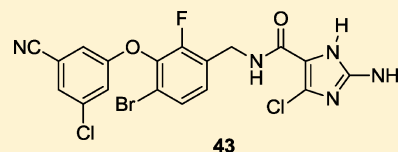
## Rational Design of Potent Non-Nucleoside Inhibitors of HIV-1 Reverse Transcriptase

Pek Chong, Paul Sebahar,<sup>†</sup> Michael Youngman, Dulce Garrido, Huichang Zhang, Eugene L. Stewart, Robert T. Nolte, Liping Wang, Robert G. Ferris, Mark Edelstein, Kurt Weaver, Amanda Mathis, and Andrew Peat\*

GlaxoSmithKline Research &amp; Development, 5 Moore Drive, Research Triangle Park, North Carolina 27709, United States

## Supporting Information

**ABSTRACT:** A new series of non-nucleoside reverse transcriptase inhibitors based on an imidazole-amide biarylether scaffold has been identified and shown to possess potent antiviral activity against HIV-1, including the NNRTI-resistant Y188L mutated virus. X-ray crystallography of inhibitors bound to reverse transcriptase, including a structure of the Y188L RT protein, was used extensively to help identify and optimize the key hydrogen-bonding motif. This led directly to the design of compound 43 that exhibits remarkable antiviral activity ( $EC_{50} < 1$  nM) against a wide range of NNRTI-resistant viruses and a favorable pharmacokinetic profile across multiple species.



## INTRODUCTION

The discovery and implementation of highly active antiretroviral therapy (HAART) in 1995 revolutionized the treatment of HIV/AIDS, significantly improving mortality rates to where it is now considered a manageable, chronic disease. Efavirenz [EFV (Figure 1a)] is a key component of HAART and acts as a non-nucleoside inhibitor of HIV-1 reverse transcriptase (RT), the enzyme responsible for conversion of viral RNA into double-stranded DNA. A concern with respect to efavirenz is its low genetic barrier for viral resistance, whereby a single-point mutation (e.g., K103N) renders the drug impotent (Table 1).<sup>1</sup> The search for second-generation NNRTIs active against efavirenz-resistant HIV-1 strains and with higher genetic barriers to resistance has yielded two additional drugs, etravirine and rilpivirine (Figure 1a and Table 1).<sup>2</sup> However, viral resistance to this mechanistic class of inhibitors continues to emerge, and there is a clear need to discover new agents with unique resistance profiles.

In the past decade, efforts at GlaxoSmithKline led to the clinical development of 2 (GW634), a prodrug of a potent non-nucleoside RT inhibitor 1 [GW248 (Figure 1b)].<sup>3</sup> Compound 2 lowered HIV-1 viral RNA titers in NNRTI-experienced patients when given as a monotherapy over 7 days.<sup>4</sup> However, there were several potential issues associated with 2 that the backup program aimed to address. First, preclinical studies revealed that the primary pathway for metabolic clearance was amide hydrolysis that liberated the corresponding carboxylic acid and aniline.<sup>5</sup> Recent studies have raised concerns around the potential toxicity associated with aromatic amines;<sup>6</sup> as such, removing the possibility of forming an aniline metabolite became a priority. Second, rash remains a major tolerability issue associated with efavirenz treatment and a liability that future drugs in this class need to address.<sup>7</sup> Although the evidence linking rash to sulfonamide functional groups remains controversial,<sup>8</sup> it seemed prudent to avoid this moiety

altogether in a backup compound. Similarly, reports that benzophenone-containing drugs can cause photosensitivity responses in patients prompted us to target analogues lacking this structural motif.<sup>9</sup> Finally, the in vitro resistance profile of 2 revealed the emergence of viruses with mutations at position 188 of HIV-1 RT.<sup>5</sup> One mutation in particular, Y188L, renders the virus resistant to many known NNRTIs, including efavirenz (Table 1).<sup>10</sup> Therefore, we focused on identifying inhibitors that would address these clinical needs.

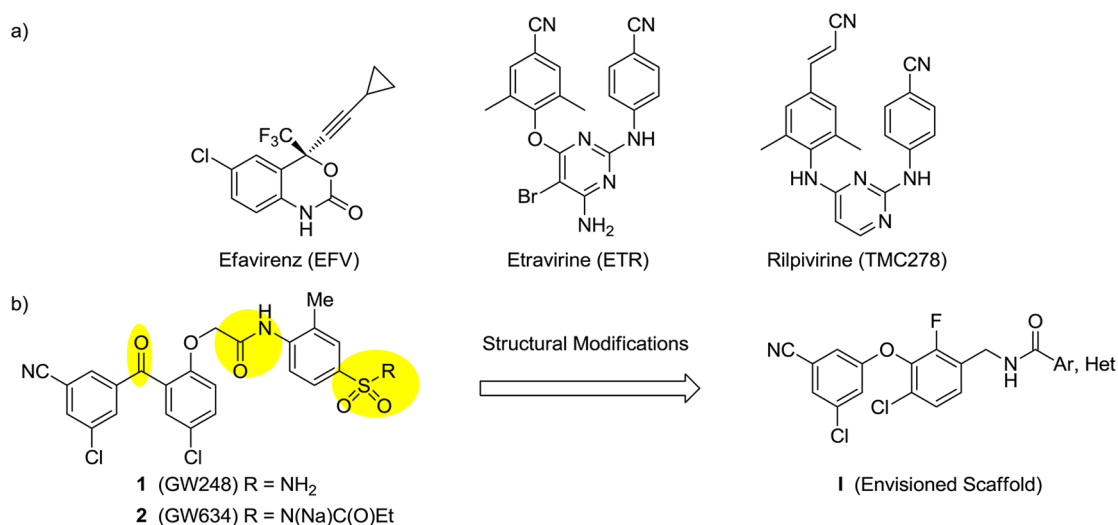
## RESULTS AND DISCUSSION

Of the desired structural changes outlined above, removal of the benzophenone group proved to be the most straightforward. In addition to our efforts,<sup>11</sup> other research groups had previously described inhibitors containing the biarylether linker that was incorporated into our design.<sup>12–14</sup> With respect to eliminating potential aniline metabolites, a simple solution was to reverse the amide connectivity, thereby leading to the envisioned target scaffold I (Figure 1b). While it was unclear if this spatial arrangement of hydrogen bond donor and acceptor would be tolerated, the potential for rapid analogue synthesis and the plethora of readily available carboxylic acids supported this approach. The requisite benzylamine 6 was prepared in eight steps with a reasonable overall yield [26% (Scheme 1)] from the commercially available phenol 3. The reactions performed well on a multigram scale, providing easily isolated intermediates and access to hundreds of grams of amine 6.

Benzylamine 6 was coupled with a diverse set of carboxylic acids to give the desired analogues in good yields.<sup>15</sup> Initial results with an aryl sulfonamide similar to the one that had improved potency within the benzophenone scaffold were disappointing, especially the absence of activity against the

Received: September 7, 2012

Published: November 8, 2012



**Figure 1.** (a) Structures of three marketed NNRTIs, efavirenz, etravirine, and rilpivirine. (b) Modification of undesirable structural features (yellow) in a prior clinical asset (2) that led to the envisioned target scaffold I.

important Y188L virus [compound 7 (Table 1)]. The benzoic acid derivatives in general failed to deliver an attractive antiviral profile, but in contrast, heteroaryl carboxamide analogues proved to be much more promising. While the 2-benzofuranyl analogue 8 also displayed poor antiviral activity, a modest improvement was noted with the 2-indole and 2-benzimidazole derivatives (9 and 10, respectively), suggesting that a hydrogen bond donor adjacent to the amide linker was advantageous. This observation was supported by analogues 11 and 12, in which removal of the hydrogen bond donor via *N*(1)-methylation of the imidazole (11) resulted in a >10-fold loss of potency versus the des-Me analogue (12).

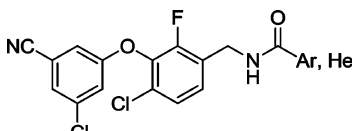
The similar activity between benzimidazole 10 and imidazole 12 was encouraging because the latter possessed improved physicochemical properties with respect to molecular weight and lipophilicity [*cLogP* (Table 1)]. A strong emphasis has been placed on improving the physicochemical properties of drug candidates as a means of reducing attrition in late stage clinical development.<sup>16</sup> Substitution at the 4-position of the imidazole ( $R_1$ ) with a Me group (13) led to a slight improvement in potency compared to that of protio analogue 12; however, introduction of an electron-withdrawing  $CF_3$  group (14) afforded a compound with subnanomolar potency versus WT and K103N viruses. More importantly, activity against the Y188L virus was also achieved. Replacing the  $CF_3$  substituent with other small electron-withdrawing groups such as Cl and Br (15 and 16, respectively) led to >45-fold increases in Y188L activity and antiviral profiles that surpassed that of the previous clinical candidate, 1. Both compounds display subnanomolar activity against another common mutation in HIV-1, Y181C, which confers NNRTI resistance.

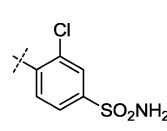
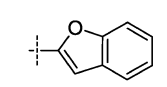
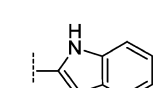
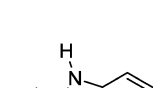
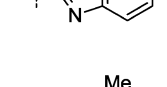
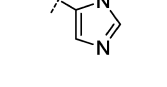
An X-ray crystal structure of analogue 15 bound to HIV-1 reverse transcriptase (Figure 2) shows the existence of two optimal H-bonds between (a) the carbonyl of the imidazole carboxamide and the amide NH group of Lys103 (2.9 Å) and (b) the imidazole NH group and the carbonyl of Lys103 (2.8 Å). The two-point binding motif explains the enhanced potency observed for heterocycles bearing an NH group adjacent to the amide carbonyl versus those without (compare compounds 9, 10, and 12–16 to compounds 8 and 11). It also explains the lack of resistance to the K103N mutation because these inhibitors hydrogen bond to NH and C=O groups

located along the protein backbone and not with the amino acid side chain. As shown in Figure 2, the Lys103 side chain is oriented away from the inhibitor and shows little change in orientation upon being mutated to Asn103.

The beneficial effect on potency resulting from substitution at the imidazole 4-position appears to be multifaceted. Small, lipophilic groups such as Me,  $CF_3$ , Cl, and Br groups (examples 13–16, respectively) occupy a small, hydrophobic pocket created by P225, F227, and P236 (Figure 2), thereby providing enhanced binding affinity over the 4-H analogue 12. The superior activity of the analogues bearing electron-withdrawing groups (14–16) versus the analogue with an electron-donating group (13) may be in part attributed to the lower  $pK_a$  of the imidazole (NH) proton. The measured  $pK_a$ 's of the imidazoles of analogues 15 and 13 are 8.9 and >12, respectively.<sup>17</sup> Increased acidity facilitates hydrogen bonding and results in stronger binding of the inhibitor to the protein backbone.

Another factor contributing to the increased activity observed with electron-withdrawing versus electron-donating groups at the imidazole 4-position is an energetic preference for a conformation conducive for binding to reverse transcriptase. A number of rotameric and tautomeric conformations are available to the imidazole-5-carboxamide derivatives; however, binding to RT requires a linear arrangement of a hydrogen bond acceptor (C=O) and donor (NH). Experimental and computational methods have shown that substitution of the 4-position of imidazoles with electron-withdrawing groups favors the conformation desired for RT binding.<sup>18,19</sup> To explore this hypothesis in the context of our lead series, we conducted ab initio calculations on a related molecule, 4-chloro-*N*-ethylimidazole-5-carboxamide, to assess the relative energies of probable conformational and tautomeric forms (Figure 3a). The results show that the conformation required for RT binding, A, is the lowest-energy conformation, being 3.4, 8.6, and 10.6 kcal/mol lower in energy than conformations C, B, and D, respectively.<sup>20</sup> This is expected as conformer A appears to minimize destabilizing steric and electronic interactions apparent in the other conformations. Conversely, ab initio calculations with the analogous Me-substituted analogue reveal that RT active conformation E is not the most stable but has 3.4 kcal/mol more energy than conformation G (Figure 3b). Taken together, the results may account for the 24–72-fold

Table 1. Antiviral Potencies and cLogP Values of Aryl and Heteroaryl Analogues<sup>a</sup>


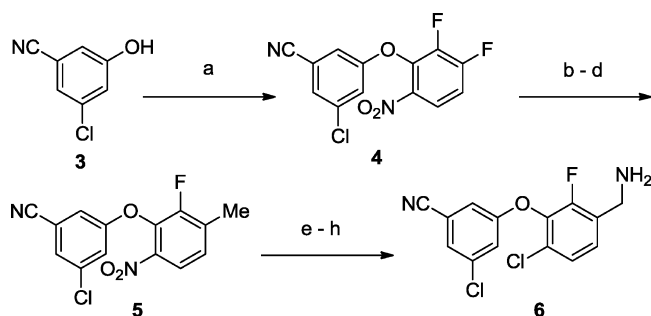
Cmpd	Ar, Het	R <sub>1</sub>	WT	EC <sub>50</sub> (nM) <sup>a</sup>			cLogP <sup>b</sup>	
				K103N	Y181C	Y188L		
EFV			0.5	20	1.0	157	3.7	
ETR			0.6	0.4	2.4	0.9	5.0	
TMC278			0.5	0.5	1.3	3.7	5.5	
1			0.3	0.5	0.5	18	3.4	
7			13	60	180	>1000	4.2	
8			52	380	340	>1000	6.1	
9			8.9	26	58	>1000	6.1	
10			5.1	18	27	>1000	6.4	
11			120	460	>1000	>1000	4.4	
12			H	9.7	48	260	>1000	4.4
13		Me	2.4	7.2	15	>1000	4.4	
14		CF <sub>3</sub>	0.1	0.7	1.4	320	4.2	
15		Cl	0.1	0.1	0.2	5.6	4.4	
16		Br	0.1	0.1	0.2	7.1	4.4	

<sup>a</sup>For details of the assay, see ref 3. Standard deviations are listed in the Supporting Information. <sup>b</sup>cLogP was calculated using the model provided in Daylight/BioByte.

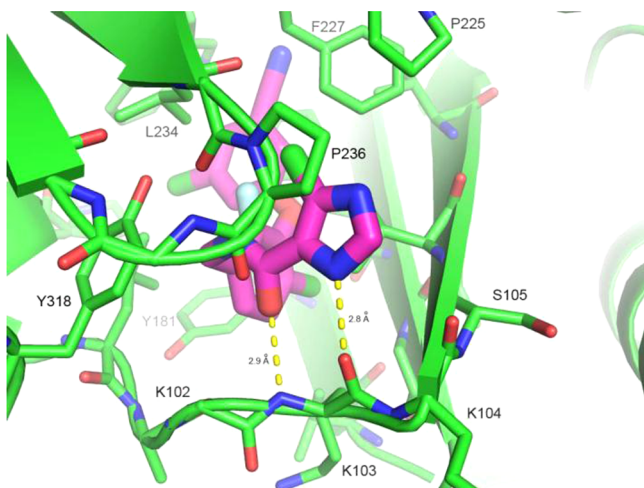
decrease in the activity of 4-Me-substituted compound **13** relative to that of 4-chloro analogue **15** against wild-type and K103N viruses.

Further investigation of the SAR required the syntheses of 4-chloro-imidazole-5-carboxylic acids with substitution at the 2-

position. Simple alkyl groups were introduced via de novo construction of the chloro-imidazole ring system according to published reports (Scheme 2).<sup>21</sup> Benzyloxyacetaldehyde **17** was subjected to standard Strecker reaction conditions, and the resulting aminonitrile was N-acylated with several acid chlorides

Scheme 1. Synthesis of the Requisite Benzylamine Intermediate 6<sup>a</sup>

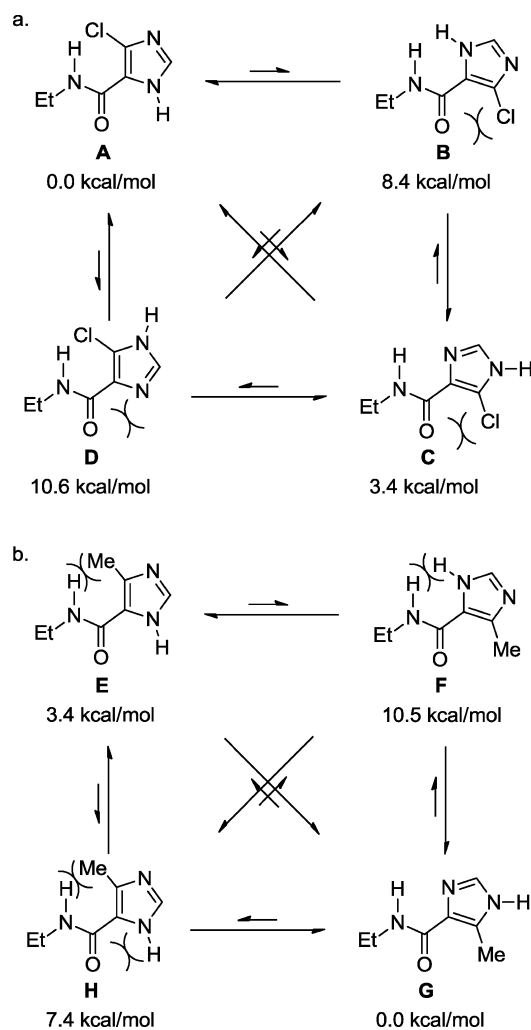
<sup>a</sup>Reagents and conditions: (a) 1,2,3-trifluoro-4-nitrobenzene, NaH, THF (74%); (b) di-*tert*-butylmalonate, NaH, THF; (c) TFA, DCM; (d) CuO,  $\Delta$ , MeCN (87% over three steps); (e) Na<sub>2</sub>S<sub>2</sub>O<sub>4</sub>, water/THF (92%); (f) CuCl<sub>2</sub>, *t*BuONO, MeCN (67%); (g) NBS, AIBN, CCl<sub>4</sub> (79%); (h) NH<sub>3</sub>, MeOH (84%).



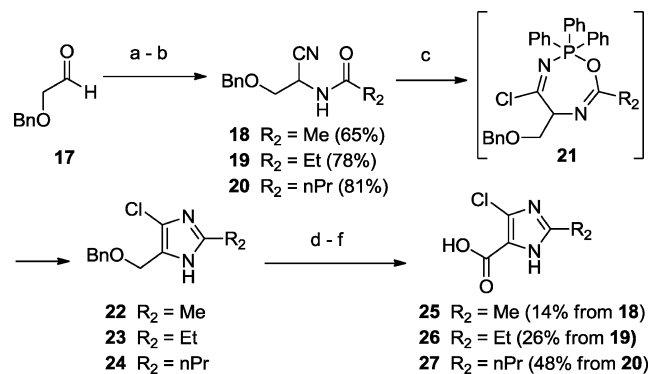
**Figure 2.** Two key binding interactions exist between compound 15 and the backbone NH and C=O groups of Lys103 of HIV-1 RT.

in good yields. Heating the *N*-acylated  $\alpha$ -aminonitriles 18–20 in the presence of PPh<sub>3</sub> and CCl<sub>4</sub> cleanly afforded chloroimidazoles 22–24, presumably via intermediate 21.<sup>21</sup> Acid cleavage of the *O*-benzyl protecting groups liberated the primary alcohols that were converted to the desired carboxylic acids 25–27 via a two-step protocol that avoided issues of imidazole oxidation. The acids were coupled with benzylamine 6 to give the desired final products 28–30 (Table 2).

Unfortunately, the cyclization of  $\alpha$ -aminonitriles was found to have a limited scope and could not be adapted to incorporate a number of other functional groups at the 2-position. To further expand the SAR within this series, a more straightforward approach involving the direct functionalization of the imidazole ring system was explored. Commercially available 2-bromo-4,5-dichloroimidazole was SEM-protected (compound 31) and then subjected to a one-pot, sequential lithiation–trapping protocol (Scheme 3). Addition of *n*-BuLi at  $-78$  °C effected halogen–metal exchange at the 2-position, and the resulting anion was trapped with 1 equiv of an electrophile (TMS-Cl<sup>22</sup> or MeSSMe). Addition of an additional 1 equiv of *n*-BuLi afforded a second halogen–metal exchange that was directed exclusively to the chlorine adjacent to the SEM-protecting group.<sup>23</sup> Subsequent treatment with DMF gave good

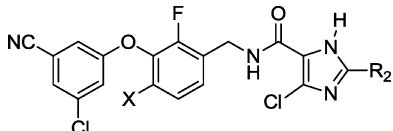


**Figure 3.** Relative energies for probable conformations of (a) 4-chloro- and (b) 4-methyl-*N*-ethyl-imidazole-5-carboxamide as calculated using ab initio methods.<sup>20</sup>

Scheme 2. Syntheses of 2-Alkyl-4-chloroimidazole Carboxylic Acids<sup>a</sup>

<sup>a</sup>Reagents and conditions: (a) NaCN, NH<sub>4</sub>Cl, NH<sub>4</sub>OH; (b) R<sub>2</sub>C(O)Cl; (c) PPh<sub>3</sub>, CCl<sub>4</sub>, MeCN,  $\Delta$ ; (d) MsOH, CHCl<sub>3</sub>; (e) MnO<sub>2</sub>, DCM, 1,4-dioxane,  $\Delta$ ; (f) NaClO<sub>2</sub>, NaH<sub>2</sub>PO<sub>4</sub>·H<sub>2</sub>O, 2-Me-2-butene, *t*BuOH, THF.

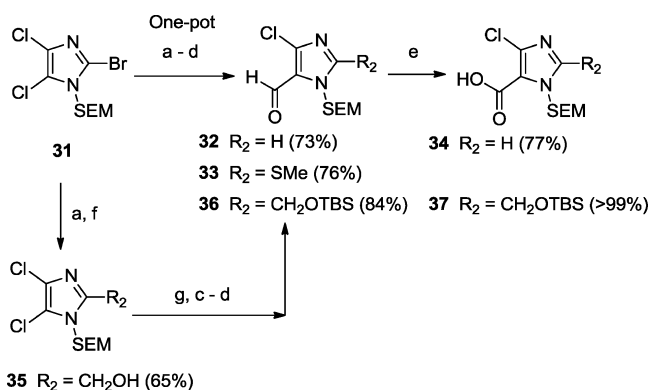
isolated yields of aldehydes 32 and 33, the former of which was oxidized to the corresponding carboxylic acid 34. Although two low-temperature metalation steps were required, this procedure

**Table 2. Antiviral Activities and cLogP Values of Imidazoles Substituted at R<sub>2</sub>**


compd	X	R <sub>2</sub>	EC <sub>50</sub> (nM) <sup>a</sup>				cLogP <sup>b</sup>
			WT	K103N	Y181C	Y188L	
15	Cl	H	0.1	0.1	0.2	5.6	4.4
28	Cl	Me	0.2	0.2	0.3	11	4.6
29	Cl	Et	0.3	0.3	0.8	76	5.2
30	Cl	nPr	0.3	0.4	1.3	240	5.7
38	Cl	CH <sub>2</sub> OH	0.3	0.3	1.2	24	3.3
40	Cl	OH	5.3	14	57	>1000	4.7
42	Cl	NH <sub>2</sub>	0.1	0.1	0.1	0.9	4.1
43	Br	NH <sub>2</sub>	0.1	0.1	0.1	0.5	4.2

<sup>a</sup>For details of the assay, see ref 3. Standard deviations are listed in the Supporting Information. <sup>b</sup>cLogP was calculated using the model provided in Daylight/BioByte.

### Scheme 3. One-Pot Sequential Lithiation and Trapping of SEM-Protected 2-Bromo-4,5-dichloroimidazole<sup>a</sup>



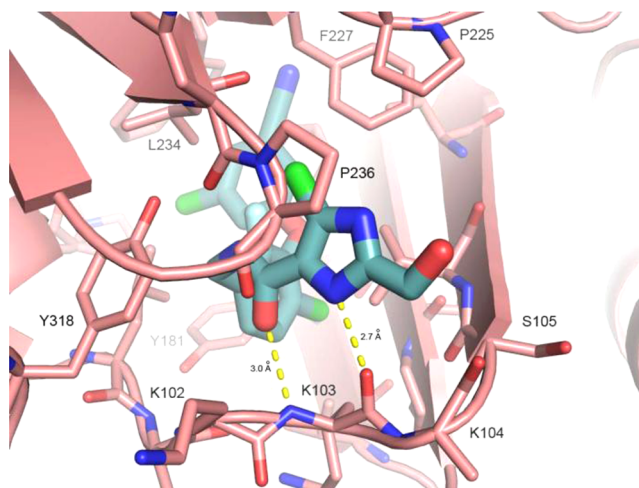
<sup>a</sup>Reagents and conditions: (a) *n*-BuLi, THF, −78 °C; (b) TMS-Cl or MeSSMe; (c) *n*-BuLi, THF, −78 °C; (d) DMF; (e) NaClO<sub>2</sub>, NaH<sub>2</sub>PO<sub>4</sub>·H<sub>2</sub>O, 2-Me-2-butene, *t*BuOH, THF; (f) (CHO)<sub>*n*</sub>; (g) TBSCl, imidazole, DCM.

was used to prepare multigram quantities of 34 (and ultimately 15) and proved to be superior to other methods aimed at directly chlorinating the imidazole. For example, attempts to chlorinate imidazole-5-carboxylic acid methyl ester using NCS gave low yields (<20%) of the desired product. The sequential lithiation protocol also provided access to 4-bromo-imidazole-5-carboxylic acids (e.g., compound 16) by employing SEM-protected 2,4,5-tribromo-imidazole as the starting material.

The treatment of the 2-lithiated imidazole with other electrophiles allowed for the incorporation of a polar functionality as in the case of paraformaldehyde, whereby the corresponding methyl alcohol 35 was formed in 65% yield (Scheme 3). The alcohol was protected as the TBDMS-ether and then treated with an *n*-BuLi/DMF mixture to give aldehyde 36. Oxidation to the corresponding acid 37, coupling to benzylamine 6, and removal of protecting groups afforded the final compound 38 (Table 2).

As shown in Table 2, increasing the size of the alkyl substituents at the 2-position of the imidazole (Me, Et, and *n*Pr) resulted in a progressive decrease in activity against the

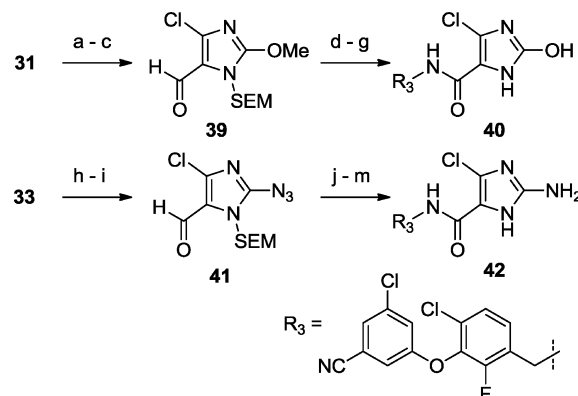
Y188L virus (examples 28–30, respectively). The deleterious effects of hydrophobic groups in this region of the molecule were not surprising given that these substituents project directly toward the solvent. Unfortunately, appending a polar 2-hydroxymethyl group (38) did not improve activity compared to that of the 2-methyl variant (28). The X-ray crystal structure of 38 bound to HIV-1 RT showed the methyl-alcohol projecting into solvent with no direct interactions with the protein (Figure 4), suggesting that while such substitution



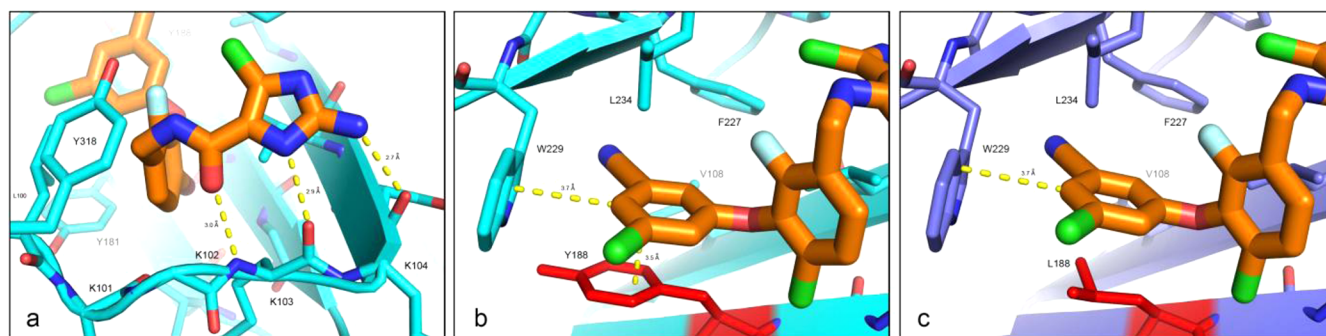
**Figure 4.** Polar hydroxymethyl group of 38 that extends past the carbonyl of K104 and projects into the solvent.

might provide a means of improving aqueous solubility, it was unlikely to significantly contribute to antiviral potency. However, it appeared that an H-bond donor directly attached to the 2-position of the imidazole might be able to interact with the backbone carbonyl group of residue 104. On the basis of this hypothesis, the 2-OH and 2-NH<sub>2</sub> analogues were synthesized (Scheme 4).

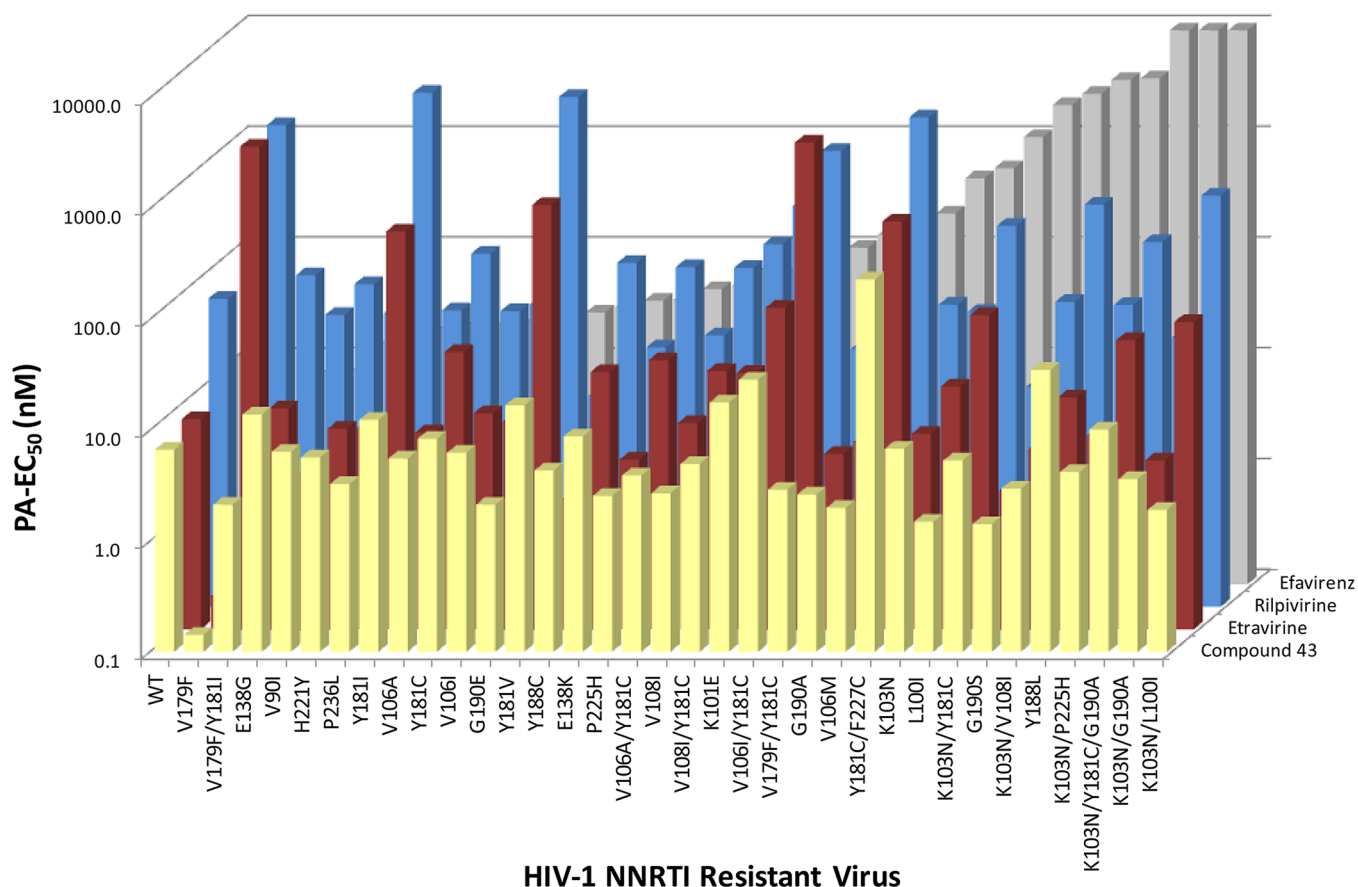
### Scheme 4. Syntheses of 2-OH- and 2-NH<sub>2</sub>-Substituted Imidazoles 40 and 42<sup>a</sup>



<sup>a</sup>Reagents and conditions. Synthesis of 40: (a) NaOMe, CuBr (67%); (b) *n*-BuLi, THF, −78 °C; (c) DMF (80%); (d) NaClO<sub>2</sub>, NaH<sub>2</sub>PO<sub>4</sub>·H<sub>2</sub>O, 2-Me-2-butene, *t*BuOH, THF (quantitative); (e) EDC, HOBT, 6, DMF; (f) TFA, DCM (56% over two steps); (g) BBr<sub>3</sub>, DCM (15%). Synthesis of 42: (h) mCPBA; (i) NaN<sub>3</sub>, DMF (69% over two steps); (j) NaClO<sub>2</sub>, NaH<sub>2</sub>PO<sub>4</sub>·H<sub>2</sub>O, 2-Me-2-butene, *t*BuOH, THF (quantitative); (k) TFA, DCM; (l) EDC, HOBT, 6, DMF; (m) Lindlar catalyst, H<sub>2</sub> (50 psi), EtOAc (53% from 41).



**Figure 5.** X-ray structure of compound 43 with HIV-1 RT that highlights (a) three-point binding of the amino-imidazole-amide with residues K103 and K104 (wild-type RT), (b)  $\pi$ -stacking and T-stacking of the terminal aryl ring of compound 43 with Tyr188 and Trp229 (wild-type RT), and (c) loss of the favorable  $\pi$ -stacking interaction upon mutation of tyrosine to leucine at position 188 (Y188L RT).



**Figure 6.** Protein-adjusted EC<sub>50</sub>'s (PA-EC<sub>50</sub>) of compound 43 relative to those of the marketed NNRTI drugs efavirenz, etravirine, and rilpivirine against a diverse set of NNRTI-resistant HIV-1 viruses. The EC<sub>50</sub> values and protein shift values are reported in the Supporting Information.

Initial results were perplexing in that 2-OH compound **40** displayed no activity against the Y188L virus while 2-NH<sub>2</sub> derivative **42** remains one of the most potent compounds we have tested. However, upon further examination, solution-phase FT-IR experiments revealed that 2-OH analogue **40** exists almost entirely as the keto tautomer.<sup>24</sup> Consequently, the imidazolone oxygen is in the proximity of the carbonyl oxygen of residue 104, and the ensuing electronic repulsion likely accounts for the large decrease in potency. In contrast, the 2-NH<sub>2</sub> group exists as the amino tautomer that is capable of hydrogen bonding with residue 104, leading to an improvement in the Y188L antiviral potency versus that of the 2-protio analogue (compare **15** to **42** in Table 2).

The optimized 2-NH<sub>2</sub>-imidazole moiety was also combined with other modified benzylamine intermediates (see the Supporting Information for synthetic details). One minor modification in which the chloro substituent was replaced with bromo on the central aromatic ring led to a further, albeit modest, improvement in potency versus that of the Y188L virus [compound **43** (Table 2)]. An X-ray crystal structure of compound **43** bound to RT protein shows the existence of three optimal H-bonds (Figure 5a). In addition to the two hydrogen bonds to Lys103 described above (3.0 and 2.9 Å), a third interaction exists between the imidazole 2-amino group and the carbonyl of Lys104 (2.7 Å).

Table 3. In Vivo Pharmacokinetic Profile of Compound 43

species	iv <sup>a</sup>			po <sup>b</sup>	
	Cl (mL/min/kg)	Vdss (L/kg)	t <sub>1/2</sub> (h)	AUC <sub>0-∞</sub> (ng/h/mL)	%F
mouse <sup>c</sup>	8.2	2.1	3.1	9605	94
rat <sup>d</sup>	28.6 ± 5.4	3.6 ± 0.4	2.2 ± 0.3	2509	84
dog <sup>e</sup>	2.8 ± 0.1	0.9 ± 0.03	4.3 ± 1.0	14277 ± 939	47 ± 3
cyno <sup>e</sup>	4.7 ± 1.3	1.8 ± 0.1	6.1 ± 1.1	6458 ± 883	34 ± 5

<sup>a</sup>Dosed intravenously at 1 mg/kg in a 10:10:80 DMSO/Solutol/5% mannitol mixture. <sup>b</sup>Dosed orally at 5 mg/kg in a 10:10:80 DMSO/Solutol/5% mannitol mixture. <sup>c</sup>Composite sampling; each time point represents  $n = 3$  mice. <sup>d</sup> $n = 3$  for iv;  $n = 2$  for po. <sup>e</sup> $n = 3$  for iv;  $n = 3$  for po.

The inhibitor–protein interactions appear to be highly optimized, to the point that potency is maintained against the challenging Y188L virus. For the biarylether class of NNRTIs, significant binding energy is gained through  $\pi$ -stacking (3.5 Å) of the terminal aryl ring of the inhibitor with the phenol of Tyr188 (Figure 5b). Mutation of tyrosine to leucine eliminates this favorable interaction, resulting in decreased activity for the inhibitor, often by as much as 100–1000-fold. We successfully obtained an X-ray crystal structures of Y188L RT protein,<sup>25</sup> including one with compound 43 bound to the NNRTI allosteric site that clearly shows Leu188 packing against the inhibitor aryl ring (Figure 5c). The fact that compound 43 exhibits a small shift in potency (5-fold) against the Y188L virus (relative to the WT virus) suggests that the strong H-bonds made through the imidazole carboxamide moiety are capable of compensating for the loss of the favorable  $\pi$ -stacking interactions.

The X-ray crystal structure of 43 bound to the wild-type RT allosteric pocket also reveals a T-stacking interaction (3.7 Å) between the terminal aryl ring of the inhibitor and the tryptophan ring of W229 (Figure 5b), a residue that is conserved across the NNRTI-resistant viruses. The favorable T-stacking interaction (3.7 Å) is maintained upon mutation of tyrosine 188 to leucine (Figure 5c); furthermore, the large volume of the trisubstituted terminal aryl ring helps occupy the void created by the smaller leucine side chain. These interactions between the aryl ring and the protein may explain the improved Y188L activity of 43 and the diarylpyridine (DAPY) analogues (e.g., etravirine and rilpivirine) relative to efavirenz, which places a nonaromatic cyclopropyl ring in this portion of the binding pocket. The greater torsional flexibility of the biarylether 43 compared to that of efavirenz may also allow the inhibitor to adapt to conformational changes within the NNRTI binding pocket that arise from mutations in the RT protein and thereby maintain key binding interactions and antiviral activity.

Compound 43 is active against a diverse set of NNRTI-resistant viruses containing single-, double-, and triple-point mutations that have been reported from clinical or in vitro studies. With the exception of the doubly mutated Y181C/F227C virus ( $EC_{50} = 3.2$  nM), compound 43 exhibits subnanomolar potency ( $EC_{50}$ ) against all of the NNRTI-resistant viruses tested [33 of 34 viruses (see the Supporting Information)].<sup>26</sup> However, the antiviral efficacy of NNRTIs in vivo is also dependent upon the free fraction of drug available in plasma, and therefore, the effect of plasma protein binding on in vitro potency was evaluated. The  $EC_{50}$ 's of 43 and other marketed NNRTIs versus wild-type HIV-1 were shifted in the presence of physiological concentrations of human serum albumin (40 mg/mL) and human  $\alpha$ -1 acid glycoprotein (1 mg/mL) with the following rank order: etravirine (13-fold) < efavirenz (23-fold) < 43 (71-fold) < rilpivirine (116-fold).<sup>26</sup> A

comparison of the protein-adjusted  $EC_{50}$ 's (PA- $EC_{50}$ ) for the four chemotypes across a diverse set of NNRTI-resistant viruses is shown in Figure 6.<sup>26</sup> Overall, 43 displays a remarkable resistance profile that is far superior to that of the gold standard, efavirenz, especially against the most prevalent NNRTI-resistant mutation, K103N. Furthermore, the activity of 43 is maintained against viruses bearing mutations at position 181 that have been shown to confer resistance to the DAPY analogues etravirine and rilpivirine.<sup>27</sup> For example, 43 showed a <3-fold decrease in potency against Y181I and Y181V (relative to the wild type), while etravirine and rilpivirine exhibited 83- and 76-fold changes, respectively. Compound 43 is also active against viruses bearing Y181 mutations and an additional mutation, including Y181C/K103N, Y181C/V179F, and Y181I/V179F. In contrast, etravirine and rilpivirine are less effective at inhibiting viruses with the Y181 double mutations. To the best of our knowledge, 43 represents one of the most potent NNRTIs ever described and highlights the level of antiviral activity that can be achieved with this mechanistic class of inhibitors.

The in vivo pharmacokinetic profile of compound 43 was examined across multiple species (Table 3). In general, the compound exhibited a favorable PK profile with low clearance in mouse, dog, and cynomolgus monkey and an oral bioavailability of >80% in mouse and rat. The oral exposure from a 5 mg/kg solution dose was high across all four species, resulting in drug plasma concentrations 24 h after the dose ( $C_{24}$ ) above the  $EC_{50}$  for all tested NNRTI-resistant viruses.

In summary, a new series of non-nucleoside reverse transcriptase inhibitors based on an imidazole-amide scaffold has been identified and shown to possess potent antiviral activity against HIV-1, including the resilient Y188L-mutated virus. X-ray crystallography of inhibitors bound to reverse transcriptase, including the Y188L protein, was used extensively to help identify and optimize the key H-bonding motif. This led directly to the design of compound 43 that exhibits remarkable antiviral activity against a wide range of NNRTI-resistant viruses and a favorable pharmacokinetic profile across multiple species. Subsequent studies with this compound as well as further optimization within this scaffold will be reported shortly.

## ■ ASSOCIATED CONTENT

### 📄 Supporting Information

Experimental details for the syntheses and spectroscopic characterization of the compounds in this paper and details related to cellular and in vivo studies. This material is available free of charge via the Internet at <http://pubs.acs.org>.

### Accession Codes

The X-ray crystal structure coordinates for compounds 15 and 38 (wild-type RT) and compound 43 (wild-type and Y188L

RT) have been deposited in the RCSB Protein Data Bank as entries 2YNE, 2YNG, 2YNH, and 2YNI.

## AUTHOR INFORMATION

### Corresponding Author

\*E-mail: andy.j.peat@gsk.com. Phone: (919) 483-6137.

### Present Address

<sup>†</sup>Myrexix, Inc., 305 Chipeta Way, Salt Lake City, UT 84108.

### Notes

The authors declare the following competing financial interest(s): All authors are current or former employees of GlaxoSmithKline.

## ACKNOWLEDGMENTS

We thank Doug Minnick in the Analytical Chemistry Department at GlaxoSmithKline for conducting FT-IR experiments to support this work.

## ABBREVIATIONS USED

HAART, highly active antiretroviral therapy; NNRTI, non-nucleoside reverse transcriptase inhibitor; RT, reverse transcriptase; EFV, efavirenz

## REFERENCES

- (1) Vrouenraets, S. M. E.; Wit, F.; Van Tongeren, J.; Lange, J. M. A. Efavirenz: A review. *Expert Opin. Pharmacother.* **2007**, *8*, 851–871.
- (2) de Bethune, M.-P. Non-nucleoside reverse transcriptase inhibitors (NNRTIs), their discovery, development, and use in the treatment of HIV-1 infection: A review of the last 20 years (1989–2009). *Antiviral Res.* **2010**, *85*, 75–90.
- (3) (a) Ferris, R. G.; Hazen, R. J.; Roberts, G. B.; St. Clair, M. H.; Chan, J. H.; Romines, K. R.; Freeman, G. A.; Tidwell, J. H.; Schaller, L. T.; Cowan, J. R.; Short, S. A.; Weaver, K. L.; Selleseth, D. W.; Moniri, K. R.; Boone, L. R. Antiviral activity of GW678248, a novel benzophenone nonnucleoside reverse transcriptase inhibitor. *Antimicrob. Agents Chemother.* **2005**, *49*, 4046–4051. (b) Andrews, C. W.; Chan, J. H.; Freeman, G. A.; Romines, K. R.; Tidwell, J. H. Benzophenones as inhibitors of reverse transcriptase. PCT Int. Appl. WO 2001017982A1, 2001.
- (4) Becker, S.; Lelezari, J.; Walworth, C.; Kumar, P.; Cade, J.; Ng-Cashin, J.; Kim, Y.; Scott, J.; St. Clair, M.; Jones, L.; Symonds, W. Antiviral Activity and Safety of GW695634, a Novel Next Generation NNRTI in NNRTI-resistant HIV-1 Infected Patients. 3rd IAS Conference on HIV Pathogenesis and Treatment, Rio de Janeiro, Brazil, 2005, WePe6.2C03.
- (5) de Serres, M.; Moss, L.; Sigafos, J.; Seffler, A.; Castellino, S.; Bowers, G.; Serabjit-Singh, C. The disposition and metabolism of GW695634: A non-nucleoside reverse transcriptase inhibitor (NNRTI) for treatment of HIV/AIDS. *Xenobiotica* **2010**, *40*, 437–445.
- (6) Turesky, R. J. Metabolism and Biomarkers of Heterocyclic Aromatic Amines in Molecular Epidemiology Studies: Lessons Learned from Aromatic Amines. *Chem. Res. Toxicol.* **2011**, *24*, 1169–1214.
- (7) Blas-Garcia, A.; Espigues, J. V.; Apostolova, N. Twenty years of HIV-1 non-nucleoside reverse transcriptase inhibitors: Time to reevaluate their toxicity. *Curr. Med. Chem.* **2011**, *18*, 2186–2195.
- (8) Johnson, K. K.; Green, D. L.; Rife, J. P.; Limon, L. Sulfonamide cross-reactivity: Fact or fiction? *Ann. Pharmacother.* **2005**, *39*, 290–301.
- (9) Bosca, F.; Miranda, M. Photosensitizing drugs containing the benzophenone chromophore. *J. Photochem. Photobiol., B* **1998**, *43*, 1–26.
- (10) Zhang, Z.; Xu, W.; Koh, Y.; Shim, J. H.; Girardet, J.; Yeh, L.; Hamatake, R. K.; Hong, Z. A novel nonnucleoside analogue that inhibits human immunodeficiency virus type 1 isolates resistant to

current nonnucleoside reverse transcriptase inhibitors. *Antimicrob. Agents Chemother.* **2007**, *51*, 429–437.

(11) Peat, A. J.; Sebahar, P. R.; Youngman, M.; Chong, P. Y.; Zhang, H. Preparation of N-(cyanophenoxybenzyl) (hetero)aryl carboxamides as a non-nucleoside reverse transcriptase inhibitors for treating HIV infection. PCT Int. Appl. WO 2008154271A1, 2008.

(12) (a) Sweeney, Z. K.; Harris, S. F.; Arora, N.; Javanbakht, H.; Li, Y.; Fretland, J.; Davidson, J. P.; Billedeau, J. R.; Gleason, S. K.; Hirschfeld, D.; Kennedy-Smith, J. J.; Mirzadegan, T.; Roetz, R.; Smith, M.; Sperry, S.; Suh, J. M.; Wu, J.; Tsing, S.; Villasenor, A. G.; Paul, A.; Su, G.; Heilek, G.; Hang, J. Q.; Zhou, A. S.; Jernelius, J. A.; Zhang, F.; Klumpp, K. Design of Annulated Pyrazoles as Inhibitors of HIV-1 Reverse Transcriptase. *J. Med. Chem.* **2008**, *51*, 7449–7458. (b) Dunn, J. P.; Swallow, S.; Sweeney, Z. K. Non-nucleoside Reverse Transcriptase Inhibitors. PCT US20040192704A1, 2004.

(13) (a) Tucker, T. J.; Sisko, J. T.; Tynebor, R. M.; Williams, T. M.; Felock, P. J.; Flynn, J. A.; Lai, M.; Liang, Y.; McGaughey, G.; Liu, M.; Miller, M.; Moyer, G.; Munshi, V.; Perlow-Poehnelt, R.; Prasad, S.; Reid, J. C.; Sanchez, R.; Torrent, M.; Vacca, J. P.; Wan, B.; Yan, Y. Discovery of 3-{5-[(6-amino-1H-pyrazolo[3,4-b]pyridine-3-yl)-methoxy]-2-chlorophenoxy}-5-chlorobenzonitrile (MK-4965): A potent, orally bioavailable HIV-1 non-nucleoside reverse transcriptase inhibitor with improved potency against key mutant viruses. *J. Med. Chem.* **2008**, *51*, 6503–6511. (b) Saggari, S. A.; Sisko, J. T.; Tucker, T. J.; Tynebor, R. M.; Su, D.-S.; Anthony, N. J. PCT US20070021442, 2007.

(14) Jones, L. H.; Middleton, D. S.; Mowbray, C. E.; Newman, S. D.; Williams, D. H. Chemical Compounds. PCT Int. Appl. WO 2006067587A1, 2006.

(15) The structures of the final compounds were supported by <sup>1</sup>H NMR and LC–MS. Yields refer to isolated compounds that were >95% pure as determined by <sup>1</sup>H NMR and LC–MS.

(16) Meanwell, N. A. Improving Drug Candidates by Design: A Focus on Physicochemical Properties As a Means of Improving Compound Disposition and Safety. *Chem. Res. Toxicol.* **2011**, *24*, 1420–1456.

(17) The pK<sub>a</sub> values were measured using a Sirius T3 spectrophotometer according to the standard procedure. The experimentally determined pK<sub>a</sub> values for compounds **13** and **15** were in good agreement with the calculated values (12.2 and 9.5, respectively) obtained using ACD Laboratories pK<sub>a</sub> Database version 12.

(18) Charton, M. Electrical effects of ortho substituents in imidazoles and benzimidazoles. *J. Org. Chem.* **1965**, *30*, 3346–3350.

(19) Ogretir, C.; Yarliran, S. AM1 and PM3 study of the protonation tautomerization and valence tautomerization of some 4-substituted imidazoles. *THEOCHEM* **1998**, *425*, 249–254.

(20) Initial conformers and tautomers were generated by the three-dimensional conversion of two-dimensional SMILES strings using CONCORD version 6.1.1 followed by manual adjustment of the relevant dihedrals to provide the starting geometries. These four initial structures were fully optimized using GAUSSIAN03 and utilizing the standard 6-31G\*\* basis set at the restricted Hartree–Fock (RHF) level of theory. Stationary points were confirmed via a single-point frequency calculation on the fully optimized geometries using the same basis set and level of theory. Examination of the frequencies revealed that all stationary points represented minimal energy geometries.

(21) Zhong, Y.-L.; Lee, J.; Reamer, R. A.; Askin, D. New Method for the Synthesis of Diversely Functionalized Imidazoles from N-Acylated  $\alpha$ -Aminonitriles. *Org. Lett.* **2004**, *6*, 929–931.

(22) In the case of TMSCl, the TMS group acts as a transient protecting group that is cleaved during workup to afford the protio analogue.

(23) Groziak, M. P.; Wei, L. Multifunctionalization of imidazole via sequential halogen-metal exchange: A new route to purine-ring analogs. *J. Org. Chem.* **1992**, *57*, 3776–3780.

(24) Spectroscopic FT-IR data supporting the predominance of the keto tautomer are available in the Supporting Information.



(25) The first X-ray crystal structure of Y188L RT protein was reported by: Hsiou, Y.; Das, K.; Ding, J.; Clark, A. D.; Kleim, J.; Rosner, M.; Winkler, I.; Riess, G.; Hughes, S. H.; Arnold, E. Structures of Tyr188Leu Mutant and Wild-type HIV-1 Reverse Transcriptase Complexed with the Non-nucleoside Inhibitor HBY 097: Inhibitor Flexibility is a Useful Design Feature for Reducing Drug Resistance. *J. Mol. Biol.* **1998**, *284*, 313–323.

(26) The EC<sub>50</sub> values, protein binding values, and standard deviations for compound **43**, efavirenz, etravirine, and rilpivirine are listed in the Supporting Information.

(27) Azijn, H.; Tirry, I.; Vingerhoets, J.; de Béthune, M.-P.; Kraus, G.; Boven, K.; Jochmans, D.; Van Craenenbroeck, E.; Picchio, G.; Rinsky, L. T. TMC278, a Next-Generation Nonnucleoside Reverse Transcriptase Inhibitor (NRRTI), Active against Wild-Type and NNRTI-Resistant HIV-1. *Antimicrob. Agents Chemother.* **2010**, *54*, 718–727.